Climate Dynamics (1997) 13:865–882

Climate
Dynamics

Quantifying the role of biosphere-atmosphere feedbacks in climate change: coupled model simulations for 6000 years BP and comparison with palaeodata for northern Eurasia and northern Africa

D. Texier[1], N. de Noblet[1], S. P. Harrison[2], A. Haxeltine[3], D. Jolly[4], S. Joussaume[1,5], F. Laarif[2], I. C. Prentice[4], P. Tarasov[2,6]

[1] Laboratoire de Modélisation du Climat et de l'Environnement, CEA Saclay, Bâtiment 709, Orme des Merisiers, F-91191 Gif-sur-Yvette Cedex, France
[2] Dynamic Palaeoclimatology, Lund University, Box 117, S-221 00 Lund, Sweden
[3] Physical Geography, Lund University, S-22100 Lund, Sweden
[4] Global Systems Group, Department of Ecology, Ecology Building, S-223 b2 Lund, Sweden
[5] Laboratoire d'Océanographie Dynamique et de Climatologie, CNRS/ORSTOM/UPCM, Paris, France
[6] Department of Geography, Moscow State University, 119 899 Moscow, Russia

Received: 5 December 1996 / Accepted: 16 June 1997

Abstract. The LMD AGCM was iteratively coupled to the global BIOME1 model in order to explore the role of vegetation-climate interactions in response to mid-Holocene (6000 y BP) orbital forcing. The sea-surface temperature and sea-ice distribution used were present-day and CO_2 concentration was pre-industrial. The land surface was initially prescribed with present-day vegetation. Initial climate "anomalies" (differences between AGCM results for 6000 y BP and control) were used to drive BIOME1; the simulated vegetation was provided to a further AGCM run, and so on. Results after five iterations were compared to the initial results in order to identify vegetation feedbacks. These were centred on regions showing strong initial responses. The orbitally induced high-latitude summer warming, and the intensification and extension of Northern Hemisphere tropical monsoons, were both amplified by vegetation feedbacks. Vegetation feedbacks were smaller than the initial orbital effects for most regions and seasons, but in West Africa the summer precipitation increase more than doubled in response to changes in vegetation. In the last iteration, global tundra area was reduced by 25% and the southern limit of the Sahara desert was shifted 2.5 °N north (to 18 °N) relative to today. These results were compared with 6000 y BP observational data recording forest-tundra boundary changes in northern Eurasia and savana-desert boundary changes in northern Africa. Although the inclusion of vegetation feedbacks improved the qualitative agreement between the model results and the data, the simulated changes were still insufficient, perhaps due to the lack of ocean-surface feedbacks.

Correspondence to: D. Texier
E-mail: dauphin@lmce.saclay.cea.fr

1 Introduction

Pollen and macrofossil evidence from the Northern Hemisphere high latitudes show that forest vegetation extended considerably further north at 6000 years Before Present (hereafter y BP) than it does today (Hyvärinen 1976; Vasil'chuk et al. 1983; Ritchie 1987; Lozhkin 1993), reflecting a significant increase in summer temperatures and a lengthening of the growing season (Prentice et al. 1996). In some regions, the northward shift of the tundra/forest boundary was as large as 200–300 km (TEMPO Members 1996). At the same time, geomorphic and biostratigraphic evidence suggests that conditions were very much wetter than today in northern Africa and central Asia (Street and Grove 1976; COHMAP Members 1988; Petit-Maire and Page 1992; Street-Perrott and Perrott 1993; Winkler and Wang 1993). Pollen and macrofossil evidence from these regions show an expansion of moisture-demanding vegetation types into now-arid regions (Street-Perrott and Perrott 1993; Jolly et al. in press). These changes have been interpreted as reflecting an expansion of the Afro-Asian monsoon (COHMAP Members 1988).

The seasonal and latitudinal distribution of insolation at 6000 y BP was different from that of the present-day, as a consequence of changes in the Earth's orbital parameters (Berger 1988). Over the Northern Hemisphere, the insolation was increased by 5% during June–July–August (JJA) and decreased by 5% during December–January–February (DJF). Simulations with atmospheric general circulation models (AGCMs) have shown that two important consequences of the changes in insolation are high-latitude warming and the enhancement of the Afro-Asian monsoon (Kutzbach and Guetter 1986; COHMAP Members 1988; Kutzbach et al. 1993; Liao et al. 1994; de Noblet et al. 1996a; Kutzbach et al. in press; Hewitt and Mitchell 1996; Hall and Valdes 1997; Masson and Joussaume in press). However, comparisons with palaeoenvironmental data suggest that the models considerably

underestimate the magnitude of changes in these regions (Prentice et al. 1993; Jolly et al. in press; Yu and Harrison 1996). This suggests that the effects of orbital forcing on high-latitude and monsoon climates are amplified by some other mechanism.

Sensitivity experiments to changes in land surface properties (such as albedo and roughness length) as a consequence of changes in vegetation (e.g. Street-Perrott et al. 1990; Foley et al. 1994; TEMPO Members 1996; Kutzbach et al. 1996) have suggested that orbitally induced high-latitude summer warming and monsoon intensification may have been amplified by vegetation feedbacks. The recent development of coupled climate-vegetation models (Henderson-Sellers 1993; Claussen 1994; de Noblet et al. 1996b; Claussen and Gayler in press), which allow for the effects of vegetation feedbacks, provides a means to test this hypothesis. In this study, we apply the BIOME1-LMD AGCM coupled model (de Noblet et al. 1996b) to simulate an equilibrium state for the 6000 y BP climate and vegetation. We then compare the output of this coupled model at equilibrium with pollen-based reconstructions of vegetation and lake-based reconstructions of changes in moisture balance, in order to assess the degree to which incorporation of vegetation feedbacks leads to a more realistic simulation of high-latitude and monsoon climates. The models, coupling strategy, and the basis for data-model comparisons are presented in Sect. 2. The response of climate and vegetation to orbital forcing and vegetation feedbacks at 6000 y BP are quantified and compared in Sect. 3. Comparisons with palaeoenvironmental data from northern Eurasia and northern Africa are presented in Sect. 4.

2 Models and methods

2.1 The biome model

The biome model (BIOME1) reconstructs global patterns in potential vegetation physiognomy from climate (Prentice et al. 1992). In the model, the terrestrial vegetation is represented by 14 plant functional types (PFTs). Constraints on the growth and regeneration of each PFT are formulated in terms of thresholds in tolerance to coldness and dryness, and to heat, chilling and moisture requirements. The cold tolerance of plants is expressed in terms of minimum mean temperature of the coldest month. The chilling requirement is expressed in terms of the maximum mean temperature of the coldest month. The heat requirement is expressed in terms of growing-degree-days (GDD), i.e. the annual accumulated temperature over a threshold temperature (5 °C or 0 °C, depending on plant type), except in the case of grasses for which the mean temperature of the warmest month is used. The moisture requirement is expressed as the ratio of annual actual evapotranspiration and annual equilibrium evapotranspiration. In each grid cell, the model selects the set of PFTs which could exist in a given climate. A simple dominance criterion is applied to this set of PFTs, such that e.g. trees are considered to be the dominant life forms where grasses and trees can co-exist. Biomes emerge from a combination of the dominant PFTs. The number of biomes is not predetermined. However, in the present application, we use the 17 biomes originally defined by Prentice et al. (1992).

2.2 The atmospheric model

The experiments have been run with version 5.3 of the LMD AGCM (Sadourny and Laval 1984; Harzallah and Sadourny 1995). The LMD AGCM is a finite difference model. The model employs a grid that is regular in longitude and in the sine of latitude, such that each grid cell has the same area. There are 64 grid points in longitude (equivalent to 5.625°) and 50 points in latitude (equivalent to $\sim 2^\circ$ in equatorial regions and $\sim 4^\circ$ to 6° poleward of 40°). The atmosphere is divided into eleven vertical sigma levels, unevenly spaced, including four levels in the planetary boundary layer. The model is run with full seasonal cycle but no diurnal cycle for insolation. The solar radiation scheme is the algorithm of Fouquart and Bonnel (1980), the long-wave radiation scheme is from Morcrette (1991). Three condensation schemes are used in a sequential mode: large-scale condensation, moist adiabatic adjustment (Manabe and Strickler 1964), and deep convection (Kuo 1965).

Version 5.3 of the LMD AGCM incorporates the SECHIBA land-surface scheme (Ducoudré et al. 1993). In these experiments, SECHIBA has been modified to allow a more physiologically and ecologically realistic treatment of canopy conductance and seasonal variations of leaf area index (Haxeltine and Prentice 1996). The modified version of SECHIBA uses the same 17 vegetation types as in the BIOME1 model. SECHIBA allows a mosaic of vegetation types, with different land-surface characteristics, to co-exist within individual AGCM grid cells and thus can readily accept the output from BIOME1, even though BIOME1 is run on a finer grid than the AGCM.

2.3 The coupling strategy

The AGCM and the BIOME1 model are asynchronously coupled as shown in Fig. 1. Asynchronous coupling is used, as in all other coupled experiments (Henderson-Sellers 1993; Claussen 1994; de Noblet et al. 1996b) because the biome model is an equilibrium model and requires a climate averaged over several years. The BIOME1 model is run on a 0.5° grid. AGCM "anomalies" (differences between the 6 ky BP experiment and the control simulation) of mean monthly temperature, precipitation and cloudiness are interpolated to this grid and superimposed on a modern climate data set from Leemans and Cramer (1991). This procedure differs from that employed by e.g. Henderson-Sellers (1993) and Claussen (1994), where the vegetation distribution was reconstructed directly from the simulated climate at the scale of the AGCM grid. Forcing the biome model with AGCM anomalies rather than with AGCM direct outputs is expected to be more appropriate when the coupled atmosphere-vegetation experiments are to be compared with palaeoclimate data because it incorporates the effects of

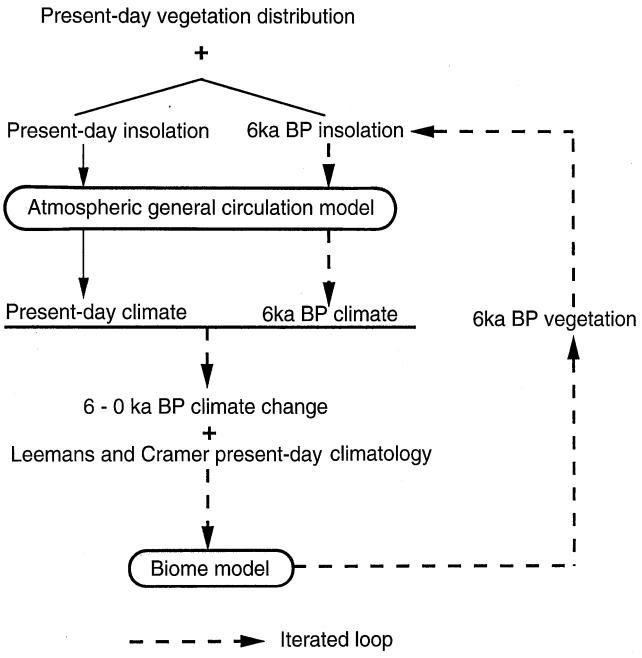

Fig. 1. Schematic diagram of the coupling between the AGCM and the biome model (BIOME1)

topography on climate, thus making it possible to capture some of the local-scale spatial pattern due to terrestrial geography (Harrison et al. 1995). The use of anomalies is also expected to minimise the systematic linear model biases (Harrison and Laarif unpublished data).

The present-day climate is simulated (control run, hereafter Ctrl) using present-day vegetation and insolation. The vegetation distribution in the control is prescribed from a BIOME1 simulation made with the modern climate data set of Leemans and Cramer (1991). In the first experiment (HOL0), the Earth's orbital parameters are set to those appropriate for 6000 y BP and CO_2 concentration is lowered from 345 ppmv to 280 ppmv, but the vegetation distribution is held constant. Thus, this experiment represents the effects of changes in insolation and CO_2 alone.

The simulated climate from HOL0 is used to drive the BIOME1 model, in order to produce a vegetation distribution appropriate to the simulated 6000 y BP climate. The daily evolution of leaf area is computed off-line from BIOME3 (Haxeltine and Prentice 1996) and depends on the ambient climatic conditions as simulated by the AGCM. Within the AGCM, the land-surface scheme SECHIBA computes the appropriate set of land-surface parameters (e.g. albedo, roughness length, canopy resistance) for each grid cell as a function of the biome type and its phenological state (see Table 1).

These changes in land-surface conditions are then used to force a new 6000 y BP simulation (HOL1) with the AGCM. This simulation represents the first iteration of the coupling, and represents the add-on effects of changes in vegetation on the 6000 y BP climate. Five iterations of the coupled model were necessary to reach an equilibrium: HOL1 through HOL5.

2.4 The simulations

Boundary conditions for the control (Ctrl) and 6000 y BP experiment (HOL0 through HOL5) are those defined for the Palaeoclimate Modelling Intercomparison Project (PMIP: Joussaume and Taylor 1995), namely: (1) orbital parameters in the control experiment were taken as those appropriate for 1950 AD and those at 6000 y BP were specified from Berger (1978); (2) the atmospheric CO_2 concentration was set to 345 ppmv for the control run and to 280 ppmv for the 6000 y BP simulations, in agreement with ice core analyses (Raynaud et al. 1993) and (3) the present-day sea-surface temperatures (SSTs) and sea-ice cover climatology of Gates (1992) were used for both the control and the 6000 y BP experiment.

The climate sensitivity to the 65 ppmv lowering in CO_2 between the control and the 6000 y BP experiments is minimised because the sea-surface parameters are prescribed as modern (Hewitt and Mitchell 1996). Simulations performed with the LMD-LMCE model (Masson personal communication) have shown that the cooling induced by the lowered CO_2, is not statistically significant and is, in any case, much smaller in magnitude than the orbitally induced changes. In terms of vegetation sensitivity, the possible physiologic effects of lowered CO_2 are not included in BIOME1.

Each simulation (Ctrl, HOL0, HOL1 through HOL5) was run for 16 years. The first year of the simulation is considered as the time necessary for spin-up, so the climate variables used as input to the BIOME1 model are a mean of the last 15 years of a simulation. This is longer than the 10-y minimum recommended in the PMIP project, but Hewitt and Mitchell (1996) have suggested that 10-y may not be long enough to get rid of the inter-annual climate variability at high northern latitudes. A 15-y mean therefore provides a better chance of obtaining statistically significant results for this region. A Student's test, at a 95% level, has been applied to annual and seasonal means of climatic variables in order to identify those regions where the climate changes are statistically significant.

Seasonal variations are discussed for climatic variables using months as defined today and therefore neglecting the changes in the length of the climatological seasons that arise from the change in earth's orbital parameters (Kutzbach and Gallimore 1988; Joussaume and Braconnot 1996). However, daily values interpolated from the monthly average of climatic variables are used for the biomes and therefore directly account for changes in the length of the seasons.

Previous experiences with asynchronous coupling (de Noblet et al. 1996b; Claussen and Gayler in press) suggest the modelled climate-vegetation system approaches quasi-equilibrium in a very few iterations (3 to 7 depending on the initial vegetation distribution). Figure 2 displays (a) the global annual mean of air temperature, and (b) the percentage of AGCM grid cells that show vegetation changes between successive iterations. Temperature decreases slightly in response primarily to changes in insolation and then to the lowering of atmospheric CO_2, but increases in response to changes in vegetation. This increase exceeds the orbitally induced cooling. A Student's

Table 1. List of the land-surface parameters prescribed and of the subsequent variables computed in the modified version of SECHIBA used for these experiments

Biome type i	Minimum albedo (%) $\alpha_{\min,i}$	Maximum albedo (%), with fresh snow $\alpha_{\max,i}$	Maximum roughness length (m) $z_{0,i}$	Canopy height (m) H_i
Polar desert	35	80	0.01	0.0
Semi-desert	25	80	0.02	0.0
Tundra	20	80	0.05	0.5
Taïga	14	20	1.0	17.0
Cold deciduous forest	14	20	0.75	15.0
Cool grass/shrub	20	80	0.05	0.5
Cool conifer forest	14	20	1.0	20.0
Cold mixed forest	14	20	0.9	20.0
Cool mixed forest	14	20	0.9	20.0
Temperate decideous forest	14	20	0.75	20.0
Evergreen/warm mixed forest	14	20	1.0	20.0
Warm grass/shrub	20	80	0.05	0.5
Hot desert	35	80	0.01	0.0
Xerophytic woods/scrub	17	50	0.5	5.0
Tropical rain forest	14	20	2.0	30.0
Tropical seasonal forest	14	20	1.0	20.0
Tropical dry forest/savanna	17	50	0.25	2.0

The daily fraction of the AGCM grid-box ($\sigma_{\text{day},i}$) that is covered by each biome is computed from the daily evolution of leaf area index (LAI), and so is the resulting fraction of non-covered soil ($f_{\text{day},i}$)

$$\sigma_{\text{day},i} = \sigma_{\max,i}(1 - \exp^{-(0.5\,LAI_{\text{day},i})})$$

$$f_{\text{day},i} = \sigma_{\max,i} - \sigma_{\text{day},i}$$

Mean daily surface albedo is computed from the albedo of each biome type:

$$\alpha_{\text{day}} = \sum_i \alpha_{\text{day},i} \quad \text{with}$$

$$\alpha_{\text{day},i} = (1 - \text{frac}_{\text{snow}}) \cdot [\sigma_{\text{day},i} + f_{\text{day},i} \cdot 1.2] + \text{frac}_{\text{snow}} \cdot \left[\alpha_{\min,i} + (\alpha_{\max,i} - \alpha_{\min,i}) \cdot \exp \frac{-\text{age of snow}}{5}\right]$$

where $\text{frac}_{\text{snow}}$ is the part of grid-box covered with snow, computed as

$\text{frac}_{\text{snow}} = \dfrac{\text{snowmass}}{\text{snowmass} + 10}$ where snowmass is the thickness of the snow layer (in cm).

Mean daily roughness length is computed from the roughness length of each biome type:

$$z_{0,\text{day}} = \exp^{\sum_i [z_{\text{day},i}]} \quad \text{with}$$

$$z_{\text{day},i} = [\sigma_{\text{day},i} \log(z_{0,i})] + [f_{\text{day},i} \log(0.7\, z_{0,i})]$$

Soil roughness length below canopy is set to 0.7 of the canopy value.
Two canopy resistances have been defined for SECHIBA (see Ducoudré et al. 1993), and are computed daily as followed:

1 An architectural resistance $= 5\sqrt{H_i LAI_{\text{day},i}}$
2 A stomatal resistance $= (1/LAI_{\text{day,e}})\, R_{\min} f(PAR) f(\delta c) f(\text{soil moisture})$

where PAR is the photosynthetically active radiation, δc the water vapour concentration deficit of the atmosphere, $LAI_{\text{day,e}}$ the effective leaf area index computed as:

$$LAI_{\text{day,e}} = 5(1 - \exp^{(-LAI_{\text{day},i}/5)})$$

and $R_{\min}$ the minimum stomatal resistance computed as:

$$R_{\min} = (1/G_{\max})(P/R\,T)$$

where $G_{\max}$ is the prescribed maximum stomatal conductance ($220\,10^{-3}$. mol. m^{-2}. s^{-1}), set to the same value for all biomes, P the surface pressure (Pa), T the surface temperature (°K) and $R = 8.314$ J. mol^{-1}. K^{-1}

test was performed on the mean seasonal climatic variables: significant differences between HOL4 and HOL5 were found to be few and scattered. Vegetation distribution is sensitive to the climate change induced by the 6000 y BP orbital forcing (Fig. 2b): 19% of the AGCM grid cells (excluding areas covered with perennial snow and ice) change vegetation. Vegetation feedbacks induce smaller changes: 11% of the cells change from HOL0 to HOL1. In subsequent iterations, the vegetation changes affect between 10 and 12% of the AGCM grid cells. Claussen (1996) obtained a similar range (9–12%) when reconstructing biome distributions from multiple 10-y

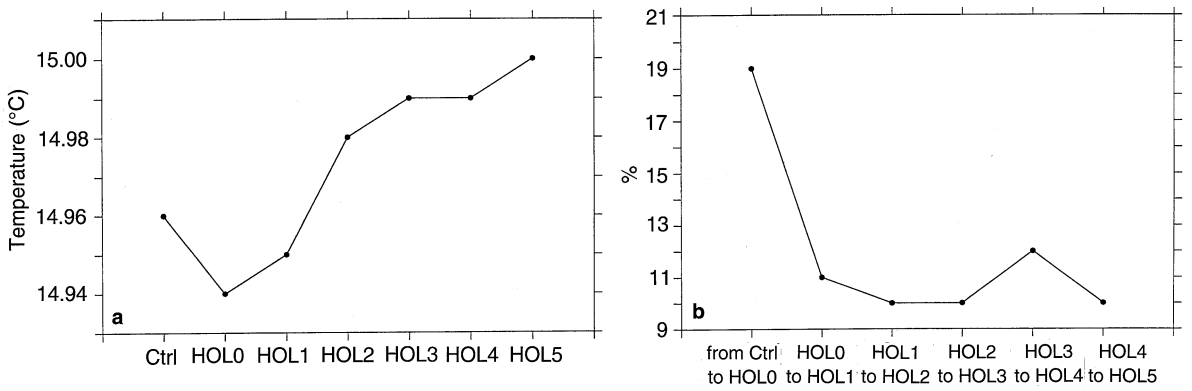

Fig. 2. **a** Global annual mean surface air temperature; **b** percentage of AGCM grid cells that change vegetation type between two successive iterations

simulated modern climatologies, suggesting that differences of this order merely reflect climate variability. These various tests suggest that HOL5 is not far from being the equilibrium state of our simulated vegetation-atmosphere system, thus running more iterations did not appear necessary. There is still some uncertainty as to how best to define the equilibrium for a coupled vegetation-atmosphere except as the absence of a "trend in global averages of land-surface parameters and climate variables" (Claussen 1994). The elaboration of an appropriate definition is beyond the scope of this study.

2.5 Palaeoenvironmental data and data-model comparison strategy

In order to test whether the introduction of vegetation feedbacks produces an amplification of the response to orbital forcing at high northern latitudes and in the monsoon zone sufficient to explain observed changes in regional climates, we have focused data-model comparisons on two regions: northern Eurasia (65 °N to pole, 0°–170 °E) and northern Africa (5°–25 °N, 20 °W–30 °E). These regions were chosen because (a) we had access to a sufficient number of palaeodata sites to allow a fairly detailed palaeoenvironmental reconstruction for 6000 y BP, (b) they are regions of relatively simple topography, faciliting comparisons with results derived from AGCM simulations, and (c) previous work (both AGCM sensitivity experiments and coupled modelling exercises) has already identified the high northern latitudes and northern Africa as areas where there is a potential for substantial biogeophysical feedbacks during the Holocene (see Sect. 4).

The position of the tundra-forest boundary at 6000 y BP across northern Eurasia has been reconstructed from pollen and macrofossil data. We have extended the compilation of pollen-derived biomes from Prentice et al. (1996), which covers northern Europe to the Urals, by adding biome reconstructions from 36 radiocarbon-dated sites from Russia (Table 2).

The expansion of the monsoon at 6000 y BP in northern Africa is reconstructed from two independent data sets: changes in lake status (a semi-quantitative measure of changes in the extent of lakes as expressed by relative water depth or lake level) and pollen-based biome reconstructions. Records of the changes in lake status at 35 sites and pollen-derived biomes from 11 sites have been derived from the compilation of Jolly et al. (in press).

The palaeoenvironmental data record climate and vegetation changes at discrete sites. It is possible to generalise such data through the use of explicit or implicit interpolation methods in order to obtain maps of past environmental conditions (e.g. Adams et al. 1990; Velichko et al. 1992; Maslin et al. 1995; Crowley 1995). However, interpolation can mask the existence of data-poor regions, and data-model comparisons using such maps can be unreliable because they place too much weight on regions with relatively sparse data (Broccoli and Marciniak 1996). Broccoli and Marciniak (1996) have recommended that evaluations of climate model simulations should be confined to the discrete sites at which palaeoenvironmental data are available; we have followed this recommendation. Thus, the site-based biome reconstructions are compared directly with the simulated vegetation distribution, and changes in lake status between 6000 y BP and present are compared with the simulated changes in precipitation minus evaporation (P–E).

3 Results

3.1 Orbitally induced changes in simulated climate and vegetation

During the mid-Holocene (6000 y BP), the seasonal contrast in insolation was greater than present over the Northern Hemisphere (NH): at the top of the atmosphere, incident solar radiation increased by 21 $W m^{-2}$ during summertime (JJA) and decreased by 10 $W m^{-2}$ during wintertime (DJF). In response to the change in summer insolation, the LMD AGCM simulates significantly warmer summers at the 95% confidence level in the NH (Fig. 3a). The summer warming is larger than 1.5 °C over most of the land north of 30 °N, reaches 2 °C over much of northern Eurasia and exceeds 2.5 °C over eastern Siberia, a region characterised by a strong inter-seasonal variability of simulated temperatures. Over the Sahel on the other hand, summer temperatures are significantly cooled by 1 °C, and by more than 2 °C over northern India and the Tibetan plateau. This simulated cooling results from the enhancement and northward expansion of the summer

Table 2. Information on the sites yielding modern and 6000 y BP vegetation data from northern Russia used in this study

Site	Latitude	Longitude	Source of evidence	Biome at 0 ka	Biome at 6 ka	Dating control[a]	Reference
Yuzhnyi (668)	70.82	57.30	Pollen	Tundra	Tundra	2D	10
Pur-Taz	66.00	79.00	Pollen	Cold deciduous forest	Taiga	1C	19
Lovozero	68.00	35.00	Pollen	Cold deciduous forest	Taiga	1D	3
Paanayarvi	66.27	30.00	Pollen	Taiga	Taiga	3D	3
Uzkoe	66.17	32.92	Pollen	Taiga	Taiga	1C	3
Baidara	68.85	66.90	Pollen	Tundra	Cold deciduous forest	1C	20
Samandon-Kazach'e	70.78	136.26	Pollen	Cold deciduous forest	Cold deciduous forest	1D	18
Yareikhoi (14/81)	68.00	60.00	Pollen	Tundra	Taiga	1D	1
Pact-6	69.34	86.70	Pollen	Cold deciduous forest	Taiga	1D	19
Kovdor	67.65	30.88	Pollen	Taiga	Taiga	4D	5
Ladonnakh G-119	72.00	96.33	Macrofossil	Tundra	Cold deciduous forest	2D	11
B. Balakhnia (A-318)	73.30	102.63	Macrofossil	Tundra	Cold deciduous forest	1D	11
B. Romanikha (XX-44)	70.82	99.08	Macrofossil	Cold deciduous forest	Cold deciduous forest	1D	11
Zakharova Rassokha	72.78	101.62	Macrofossil	Tundra	Cold deciduous forest	1D	11
Mitrofanovskoe	67.83	59.00	Pollen	Tundra	Taiga	2D	2
B. Balakhnia	73.25	100.72	Macrofossil	Tundra	Cold deciduous forest	3D	12
M. Balakhnia	72.75	103.00	Macrofossil	Tundra	Cold deciduous forest	3D	12
Kheta	70.63	94.75	Macrofossil	Cold deciduous forest	Cold deciduous forest	1D	12
Zap. Taimyr	74.53	100.50	Macrofossil	Tundra	Cold deciduous forest	1D	12
Khatanga	72.78	104.63	Macrofossil	Tundra	Cold deciduous forest	1D	12
Novaya-M. Balakhnia	72.55	103.50	Macrofossil	Tundra	Cold deciduous forest	1D	12
B. Balakhnia-27	73.37	104.35	Macrofossil	Tundra	Cold deciduous forest	2D	12
B. Balakhnia-28	73.43	100.52	Macrofossil	Tundra	Cold deciduous forest	2D	12
B. Balakhnia-29	73.31	100.53	Macrofossil	Tundra	Cold deciduous forest	2D	12
Mosun	72.78	104.22	Macrofossil	Tundra	Cold deciduous forest	3D	12
Ary-Mas	72.50	101.83	Pollen	Cold deciduous forest	Taiga	1C	16
Kuobakh-Baga	65.00	143.33	Macrofossil	Cold deciduous forest	Cold deciduous forest	1D	13
Yuribei-26	68.35	71.88	Pollen/macrofossil	Tundra	Taiga	2D	14, 15
Pukhuchayakha	71.43	67.96	Pollen/macrofossil	Tundra	Cold deciduous forest	3D	14
V. Yurubei	68.21	70.19	Pollen/macrofossil	Tundra	Taiga	2D	14
Igarka	67.43	86.58	Pollen	Cold deciduous forest	Taiga	1D	9
Duvannyi Yar	68.63	159.17	Pollen	Cold deciduous forest	Cold deciduous forest	2D	6
Dresvianka	68.45	55.26	Pollen	Tundra	Taiga	1C	17
Malaya Kheta	69.57	84.53	Macrofossil	Cold deciduous forest	Taiga	1C	7
Karginskii	69.95	83.58	Macrofossil	Tundra	Taiga	1D	4
Sypnoi Yar	68.90	147.58	Pollen	Taiga	Taiga	5D	6
Shamanovo	69.98	147.58	Pollen	Tundra	Cold deciduous forest	4D	8

[a] Dating control is a measure of the accuracy of the identification of the 6000 y BP interval, and makes use of schemes for continuous (C) and discontinuous (D) records as given in Tarasov et al. (1996). For continuous records, a dating control of 1C indicates that there are two, bracketing radiometric dates each within 2000 y of 6000 y BP; for discontinous records, a dating control of 1D, 2D, 3D, 4D or 5D indicates a radiometric date within 250, 500, 750, 1000 and 1500 y respectively of 6000 y BP

1. Bolikhovskaya et al. (1988)
2. Davydova et al. (1992)
3. Elina et al. (1995)
4. Firsov et al. (1972)
5. Kagan, Koshechkin, Lebedeva (1992)
6. Kaplina and Lozhkin (1979)
7. Kind (1974) and
8. Lavrushin et al. (1963)
9. Levkovskaya et al. (1970)
10. Malyasova and Serebriannyi (1993)
11. Nikol'skaya (1982)
12. Nikol'skaya and Cherkasova (1982)
13. Shilo et al. (1971)
14. Vasil'chuk et al. (1983)
15. Parunin et al. (1984)
16. Ukraintseva (1991)
17. Veinbergs et al. (1995)
18. Velichko et al. (1994)
19. Andreev, personal communication
20. Andreev and Tarasov, personal communication

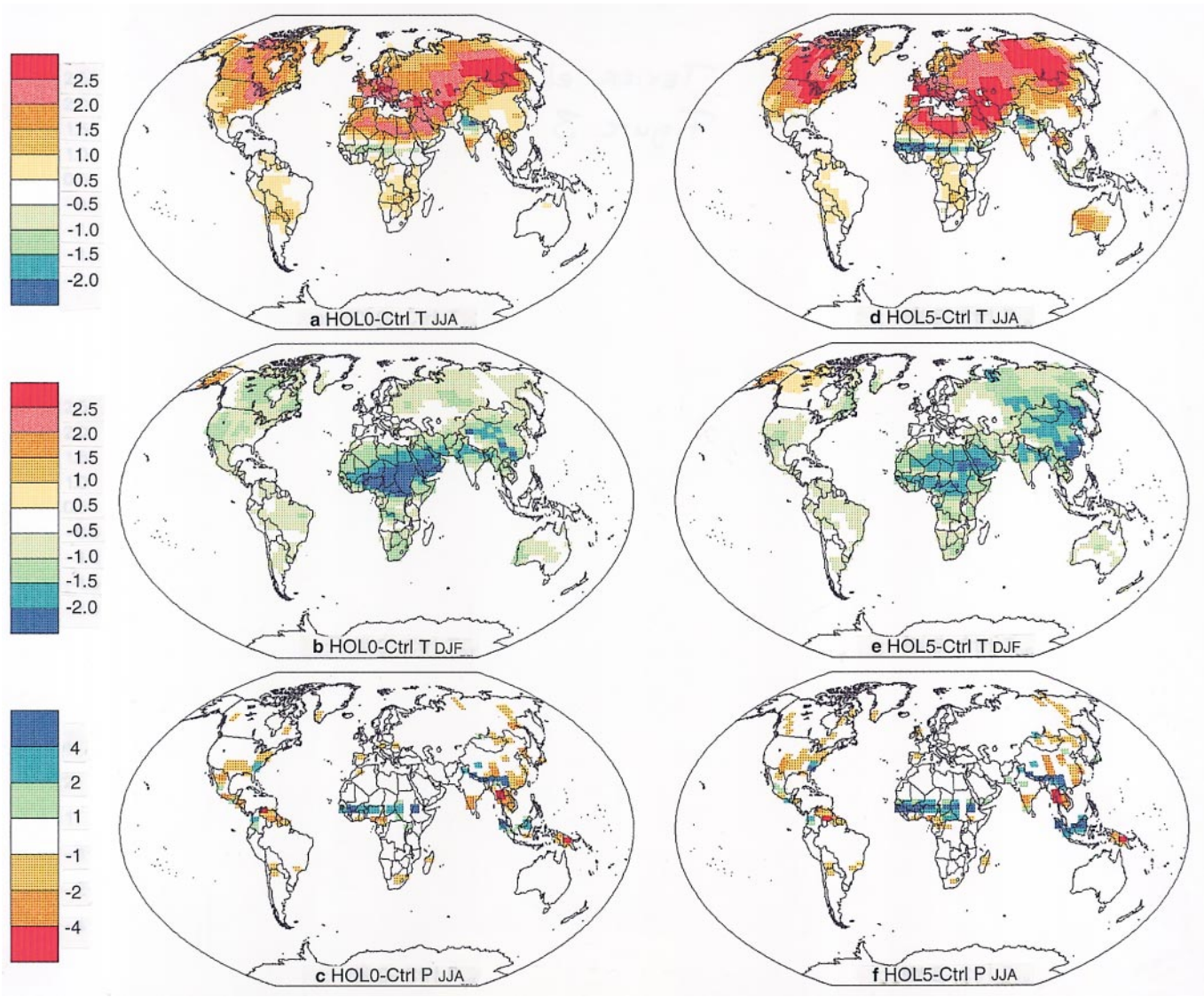

Fig. 3a–f. Climate changes simulated in response to 6000 y BP orbital forcing (HOL0-Ctrl) and to the combined effects of orbital forcing and vegetation feedbacks (HOL5-Ctrl): **a** June–July–August (JJA) surface air temperature (°C) for HOL0-Ctrl; **b** December–January–February (DJF) surface air temperature (°C) for HOL0-Ctrl; **c** JJA precipitation (mm day^{-1}) for HOL0-Ctrl; **d** JJA surface air temperature (°C) for HOL5-Ctrl; **e** DJF surface air temperature (°C) for HOL5-Ctrl; **f** JJA precipitation (mm day^{-1}) for HOL5-Ctrl

monsoons (see later) because the increased precipitation induces a significant increase in evapotranspiration and increased cloudiness; these secondary changes both cool the land.

In response to the decrease in insolation during wintertime, the LMD AGCM simulates colder winters in most of the NH (Fig. 3b) except for western Alaska where warmer winters are simulated. The magnitude of winter cooling ranges from 0.5 °C to 1.5 °C across the high and mid northern latitudes whereas winter warming ranges from 0.5 °C to 2 °C. The warming in Alaska is caused by a deepened Aleutian low which advects warm air into the region. However, the change in winter temperature north of 30 °N is not significant due to the large interannual variability of winter climate in these regions. In the tropics, there is a large and significant cooling of 2 to 3 °C across northern Africa and parts of central Asia, where the insolation change is maximal.

As a consequence of the strengthened land-sea temperature gradient in summer, the African and Asian monsoons are intensified and penetrate further inland. There is a significant increase in summer precipitation, that (in terms of regional means) exceeds 3 mm day^{-1} over the Sahel, 4 mm day^{-1} over the Tibetan plateau, and reaches 3 mm day^{-1} over Indonesia (Fig. 3c). The simulated increase in summer precipitation over the Sahel corresponds to a northward expansion of the intertropical convergence zone by about 2.5° latitude. Summer precipitation decreases over west-central Africa, southern India and Indochina, and over southeastern China. These changes in rainfall are determined by the shift in the main convergence cells: northeastward in Africa and

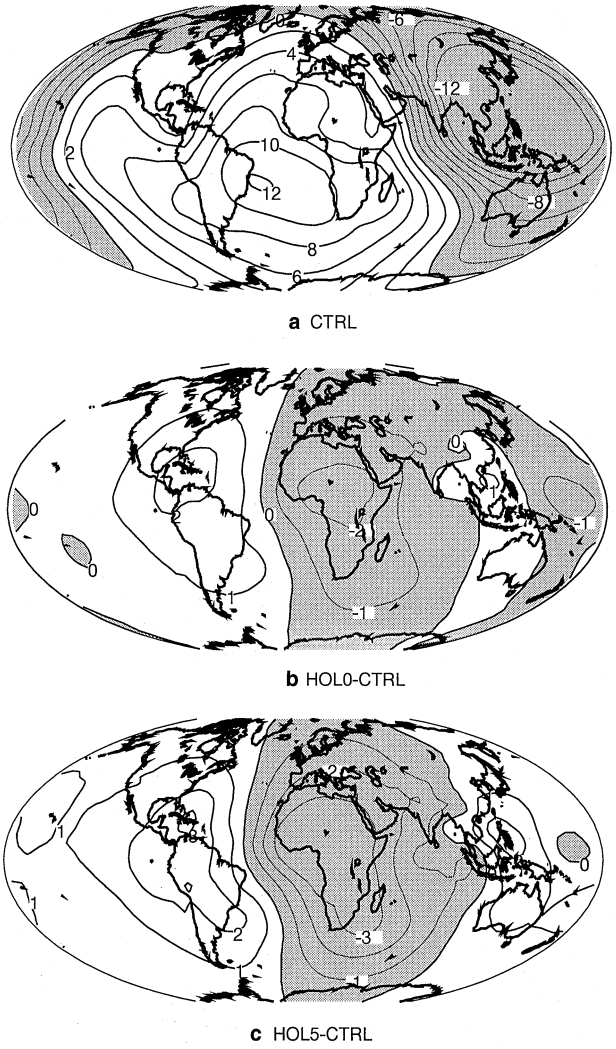

Fig. 4a–c. Mean simulated 200 hPa velocity potential ($\times 10^6\ m^2\ s^{-1}$) in June–July–August for **a** the present-day climate (Ctrl); mean change in the simulated 200 hPa velocity potential ($\times 10^6\ m^2\ s^{-1}$) in June–July–August for **b** the orbitally induced climate change (HOL0-Ctrl); **c** the orbitally and vegetation induced climate change (HOL5-Ctrl). *Negative contours* (i.e. regions with upper-level divergence) are *dashed* and *shaded*

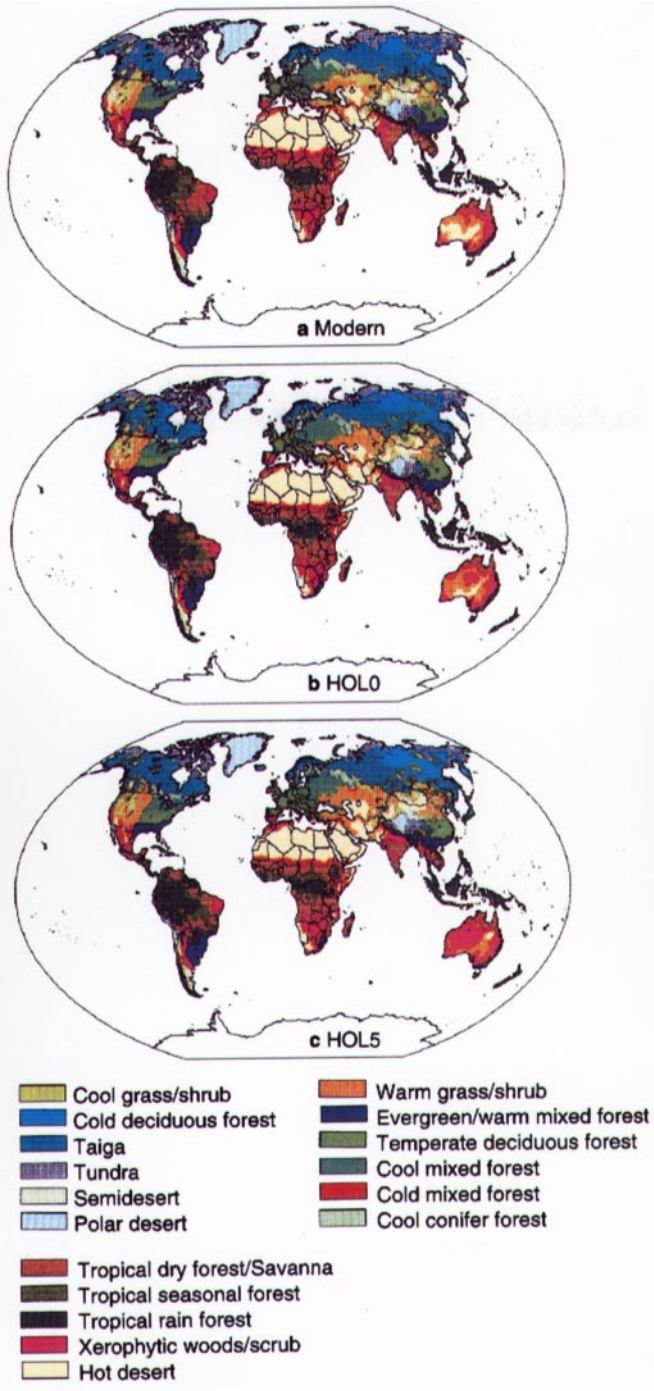

Fig. 5a–c. Simulated vegetation distribution: **a** modern, based on climatological data (Leemans and Cramer 1991); **b** from experiment HOL0, based on 6000 y BP orbital conditions and present vegetation; **c** from experiment HOL5, based on 6000 y BP orbital conditions and vegetation from HOL4

northwestward in Asia as discussed in de Noblet et al. (1996a). Indeed, Fig. 4 shows that, with orbital forcing alone the upper-level divergence (i.e. the low-level convergence) is decreased over the western Pacific and the Bay of Bengal, and increased over the Asian monsoon region and particularly over Africa. When vegetation feedbacks are included, the reinforcement of the upper-level divergence is even more pronounced.

These changes in regional climates produce a change in the distribution of terrestrial vegetation (Fig. 5b compared with Fig. 5a), the major features of which are (1) a reduction of the tundra area at high northern latitudes, (2) an expansion of warm grassland in mid-latitudes and (3) a reduction of hot desert. At high northern latitudes, summer warming leads to an increase in the length of the plant growing season resulting in a northward shift of the forest/tundra boundary. The area of tundra is reduced by 20%. In mid-latitudes, the summer warming induces a shift from cold to warm grasslands: the area of cold grassland is reduced by 31% compared to present. The simulated mid-latitude summer warming is accompanied by drier conditions and a concomitant reduction in available soil moisture. As a result warm grassland also expands into regions occupied today by boreal or temperate

forests. In the tropics, increased soil moisture allows moisture-demanding vegetation to expand. The area of hot desert is reduced by 5% in the NH. In Africa, the southern limit of the Sahara moves northward by 0.5° of latitude west of about 12 °E, and by between 1 to 2° east of about 12 °E such that the simulated area of the Sahara is reduced by 9%.

The northward shift of the treeline at high northern latitudes induces a decrease of the mean surface albedo of about 1% in summertime and 4% in the presence of snow cover (Table 3a). The largest increase in surface solar radiation reflectivity occurs during the snow season because the forests, unlike the low tundra vegetation, protrude above the snow cover and partly mask it (Federer 1968; Bonan et al. 1992; Chalita and Le Treut 1994; Foley et al. 1994). The change from tundra to forest also induces an increase in summertime vegetation roughness length by 0.12 m over the boreal latitudes and a large decrease in canopy resistance to evapotranspiration. In the mid-latitudes, the change from cold to warm grasslands does not affect land-surface characteristics in a significant way. However, the expansion of grasslands into areas now-occupied by boreal or temperate forests results in an increase in surface albedo, a decrease in roughness lengh and an increase in canopy resistance to evapotranspiration. In general, these changes only affect rather small, discrete areas and thus their subsequent impact on climate is limited. In eastern Siberia, however, the replacement of boreal forest by cold grassland significantly enhances winter cooling (see later). The expansion of moisture-demanding vegetation into the desert induces a decrease in albedo, an increase in roughness length and a decrease in canopy resistance to evapotranspiration. In northern Africa, for example, albedo decreases by 2% (Table 3b) and roughness length increases by 0.08 m.

These changes in land-surface parameters are used to drive the AGCM, in order to produce a new simulation of the 6000 y BP climate (HOL1). This procedure is iterated until HOL5. Through the successive iterations (from HOL1 to HOL5), the direction of changes in vegetation distribution are similar to those produced by orbital forcing but the magnitude of the changes decreases.

3.2 The response of climate and vegetation to 6000 y BP orbital forcing and vegetation feedbacks

The main effects of the simulated vegetation changes (ie. experiments HOL5-HOL0) are to produce (1) a surface warming throughout the year, at high and mid latitudes (Fig. 3d–e); and (2) an enhancement of the orbitally-induced summer rainfall increase (Fig. 3f) in the tropics.

Table 3. Changes in surface albedo, roughness length and canopy resistance to evapotranspiration are computed over the restricted part of the region that changes vegetation; changes in climate are computed over the entire region: **(a)** high northern latitudes: from 55 °N to 90 °N and from 180 °W to 180 °E; **(b)** northern Africa: from 5 °N to 25 °N and from 20 °W to 30 °E. Means computed over West Africa (20 °W to 12 °E) are in italic; means computed over eastern northern Africa (12 °E to 30 °E) are underlined

	Ctrl	Orbitally induced changes HOL0-Ctrl	Vegetation induced changes HOL5-HOL0	Orbitally and vegetation-induced changes HOL5-Ctrl
Surface air temperature (°C)				
JJA	19.94	+ 1.70	+ 0.42	+ 2.12
SON	− 0.66	− 0.27	+ 0.10	− 0.17
DJF	− 12.91	− 0.54	+ 0.28	− 0.26
MAM	0.39	− 0.78	+ 0.32	− 0.46
Absorbed solar radiation ($W m^{-2}$) JJA	219.17	+ 13.12	+ 1.81	+ 14.93
Latent heat flux ($W m^{-2}$) JJA	72.60	+ 3.60	+ 0.70	+ 4.30
Sensible heat flux ($W m^{-2}$) JJA	59.70	+ 6.42	+ 1.20	+ 7.62
Tundra	8080502.00 km^2	− 20.00%	− 5.00%	− 25.00%
Surface albedo (%)				
JJA	18.33	− 1.33	− 0.33	− 1.66
SON	32.00	− 3.00	− 1.33	− 3.33
DJF	48.00	− 4.00	− 2.33	− 6.33
MAM	41.66	− 4.00	− 1.66	− 5.66
Roughness length (m)				
JJA	0.28	+ 0.12	+ 0.06	+ 0.18
SON	0.27	+ 0.11	+ 0.06	+ 0.17
DJF	0.27	+ 0.11	+ 0.06	+ 0.17
MAM	0.27	+ 0.11	+ 0.06	+ 0.17
Canopy resistance to evapo-transpiration ($s m^{-1}$)				
JJA	876.84	− 61.60	− 15.73	− 77.33
SON	1643.00	− 866.10	+ 106.56	− 759.54
DJF	1019.00	− 340.00	− 612.40	− 952.40
MAM	542.10	− 233.30	+ 26.20	− 207.10

Table 3b

	Ctrl	Orbitally induced changes HOL0-Ctrl	Vegetation induced changes HOL5-HOL0	Orbitally and vegetation-induced changes HOL5-Ctrl
Annual precipitation	1.70 *1.95*/1.47	+ 0.32 + *0.34*/ + 0.24	+ 0.35 + *0.40*/ + 0.30	+ 0.67 + *0.74*/ + 0.54
Summer (JJA) precipitation ($mm\,day^{-1}$)	3.70 *4.32*/2.96	+ 0.82 + *0.73*/ + 0.66	+ 0.61 + *0.86*/ + 0.55	+ 1.43 + *1.60*/ + 1.21
Annual latent heat flux ($W\,m^{-2}$)	36.52	+ 4.20	+ 4.20	+ 8.40
Annual sensible heat flux ($W\,m^{-2}$)	56.57	− 3.86	+ 0.10	− 2.86
Annual P-E balance ($mm\,day^{-1}$)	+ 0.60	+ 0.21	+ 0.26	+ 0.47
Annual total cloud cover (%)	29.44	+ 2.84	+ 2.37	+ 5.21
Hot desert area	5 328 560.5 km^2	− 9.00%	− 10.50%	− 19.50%
Surface albedo (%) JJA	22.33	− 2.00	− 1.00	− 3.00
Roughness length (m) JJA	19.66	+ 0.08	+ 0.06	+ 0.14
Canopy resistance to evapo-transpiration ($s\,m^{-1}$) JJA	535.30	− 10.34	− 15.73	− 26.07

Incorporation of vegetation feedbacks leads to a statistically significant enhancement of the orbitally induced summer warming of about 0.5 °C over most of North America and 0.5 °C to 1.0 °C over the Eurasian high latitudes between 30° to 120°E. In southwestern Europe, northern Africa, Arabia and Central Europe, a similar enhancement of summer temperatures (0.5 °C) is simulated (Fig. 3d compared to 3a). Over northern Africa and Arabia the simulated summer warming is consequent on the strengthening of the African monsoon: increased convection in this region is, as expected, accompanied by an increase in subsiding air further north (with adiabatic warming). In the southern Sahara, the changes in roughness length and canopy resistance caused by the northward extension of sahelian vegetation induces an increase in evapotranspiration and therefore in convective rainfall (see later) leading to a cooling of the land-surface. The increase in roughness length and the decrease in canopy resistance prevail over the effects of decreasing surface albedo which would otherwise warm the surface.

In winter (DJF) and spring (MAM), the surface warming in mid and high northern latitudes results from the shading effects of tall vegetation on snow reflectivity, and reduces the orbitally-induced cooling (Table 3a). At high latitudes, the simulated extension of forested areas produce a significant winter warming over north-western America (Fig. 3e), that ranges from 0.5 °C to 2 °C compared to present. Over northern Russia on the other hand, more specifically east of the Urals and over northeastern Siberia, the orbitally induced winter cooling is enhanced despite the northward migration of the treeline, but is not significant due to the large climate variability in winter in these regions. In Mongolia winter cooling is significantly enhanced due to the intrusion of large patches of grasslands in forested areas, that induces an increase in surface albedo.

The steepened thermal gradient across northern Africa (HOL5-Ctrl compared to HOL0-Ctrl) is such that rainfall penetrates further north. Precipitation significantly increases over northern Africa by 5 $mm\,day^{-1}$ compared to the control simulation. Similar effects are seen on the Tibetan Plateau and over Indonesia, where precipitation significantly increases by 5 $mm\,day^{-1}$ and 7.5 $mm\,day^{-1}$ respectively, compared to present.

The changes in simulated climate in response to the combined effects of orbital forcing and vegetation feedbacks at 6000 y BP (i.e. HOL5-Ctrl) produce a significant change in vegetation distribution (Fig. 5c). The boreal forests expand further north, in response to the simulation of warmer summers and a longer growing season. The area of tundra is reduced by 25% of its present-day extent, compared to the 20% reduction produced by orbital forcing alone (HOL0-Ctrl). In the mid-latitudes, the area of warm grassland also expands further: the increase is 62% compared to 46% in response to orbital forcing alone. The further amplification of the summer monsoons leads to an expansion of moisture-demanding vegetation at the expense of desert. In the tropics, hot deserts are reduced by 11% compared to 8% in response to orbital forcing alone; the changes are particularly significant in northern Africa, where the Sahara is reduced by 19.5% compared to 9% in response to orbital forcing alone.

The regions which show the largest changes in vegetation distribution in response to orbital forcing (HOL0-Ctrl) and to the associated vegetation feedbacks (HOL5-HOL0) are the same (Fig. 6a–b). The magnitude of the

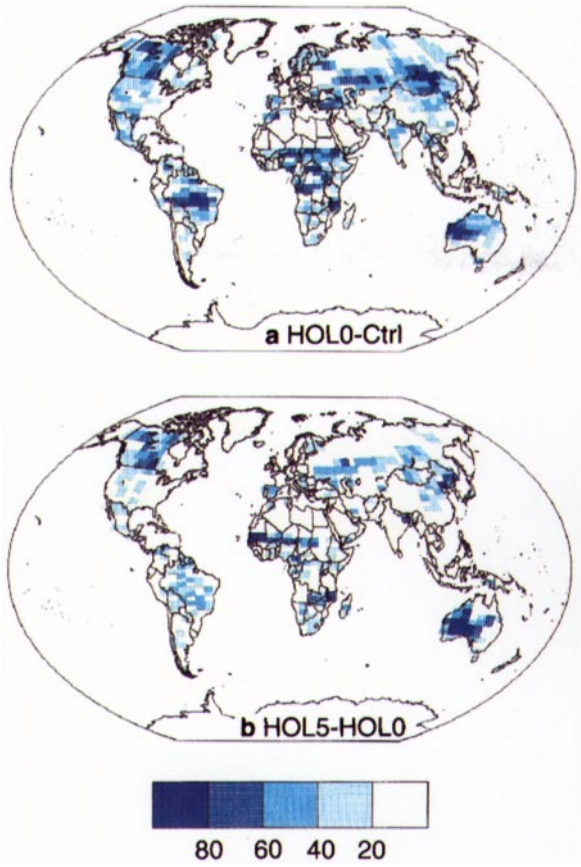

Fig. 6a, b. Percentage of an AGCM grid cell that changes vegetation cover in response to **a** 6000 y BP insolation changes (HOL0-Ctrl); **b** 6000 y BP vegetation feedbacks (HOL5-HOL0)

changes in climate and vegetation distribution as a result of the inclusion of vegetation feedbacks are generally smaller than those due to orbital forcing. Thus, orbital forcing warms the summer temperatures in the high latitudes of the NH by 1.7 °C and increases the annual precipitation over northern Africa by 0.32 mm day^{-1} relative to present; the associated vegetation feedbacks produce an additional summer warming of 0.42 °C and an increase in the African annual precipitation of 0.35 mm day^{-1} (Table 3a–b). The orbitally induced climates change reduce the tundra by 20% and the tropical hot deserts by 8% of their present-day area; the tundra area is reduced by a further 5% and the hot deserts by a further 3% when vegetation feedbacks are taken into account. The greater sensitivity to orbital forcing than to vegetation feedbacks is also reflected in the overall magnitude of vegetation change in response to orbital forcing and vegetation feedbacks (Fig. 6a–b). In the mid-latitudes of Eurasia, for example, there are large areas where more than 20% of each grid cell undergoes a change in vegetation cover in response to orbital changes and peak values are more than 60% (Fig. 6a); the area with values of more than 20% change is smaller in response to vegetation feedbacks and peak values are always less than 60% (Fig. 6b). A similar situation occurs in the tropics, where the area with values of less than 40% is larger in response to orbital changes than in response to vegetation feedbacks.

However, there are specific regions where the vegetation response to vegetation feedbacks is larger than the response to orbital forcing. On the West African coast, for example, the change in vegetation distribution as a consequence of orbital changes affects less than 20% whereas the change due to vegetation feedbacks affects more than 80% of each grid cell. To the west of Lake Chad, orbital forcing alone produces an increase in summer precipitation of 0.73 mm day^{-1} whereas vegetation feedbacks produce a further increase of 0.86 mm day^{-1} (Table 3b). In terms of annual means, the magnitude of the rainfall increase induced by vegetation feedbacks is stronger than the orbitally induced signal, over the whole of northern Africa (Table 3b). The potential importance of vegetation feedbacks in certain regions is emphasised by data-model comparisons, dealt with in the following section, which show that coupled model simulations still underestimate the observed vegetation shifts.

4 Data-model comparisons

4.1 Northern Eurasia

The data show a significant northward shift of forest biomes at 6000 y BP (Fig. 7d–e). In northern Scandinavia, the modern vegetation of tundra and taiga was replaced by cold mixed forest and cold deciduous forest. In western Siberia, taiga extended northward to the Arctic coast into regions now occupied by tundra. In eastern Siberia, the tundra was replaced by cold deciduous forest. Of the available sites from Russia, only three register tundra vegetation at 6000 y BP (Table 2).

According to the simulated biome maps, orbital changes produce a northward shift of the tundra-forest boundary (HOL0: Fig. 7b). In the west, taiga replaced tundra in response to the simulated increase in the length of the growing season. In the east, the simulation of cold winters prevented the expansion of boreal evergreen conifers, and thus the simulated increase in the growing season is registered by an expansion of cold deciduous forest. The increase in the area of cool grass/shrub in eastern Siberia (Fig. 7b) is a consequence of the simulated increase in aridity. The incorporation of vegetation feedbacks (HOL5: Fig. 7c) results in a further northward migration of the treeline, particularly in central and eastern Siberia, and a further expansion of cool grass/shrub in eastern Siberia. In Scandinavia, a slight winter warming leads to the expansion of cool conifer forest at the expense of taïga. However, the changes due to vegetation feedbacks are small compared to those produced by orbital forcing alone. Thus, orbital forcing alone leads to a reduction of tundra by 27% in this region compared to present, while the combined effects of orbital forcing and vegetation feedbacks results in a reduction of tundra to 34% of its modern extent.

The simulated changes in the position of the treeline in response to orbital changes is qualitatively in agreement with the palaeoenvironmental data, but significantly underestimates the magnitude of the northward shift in central Siberia. The incorporation of vegetation feedbacks produces a further shift in the tundra-forest boundary, but

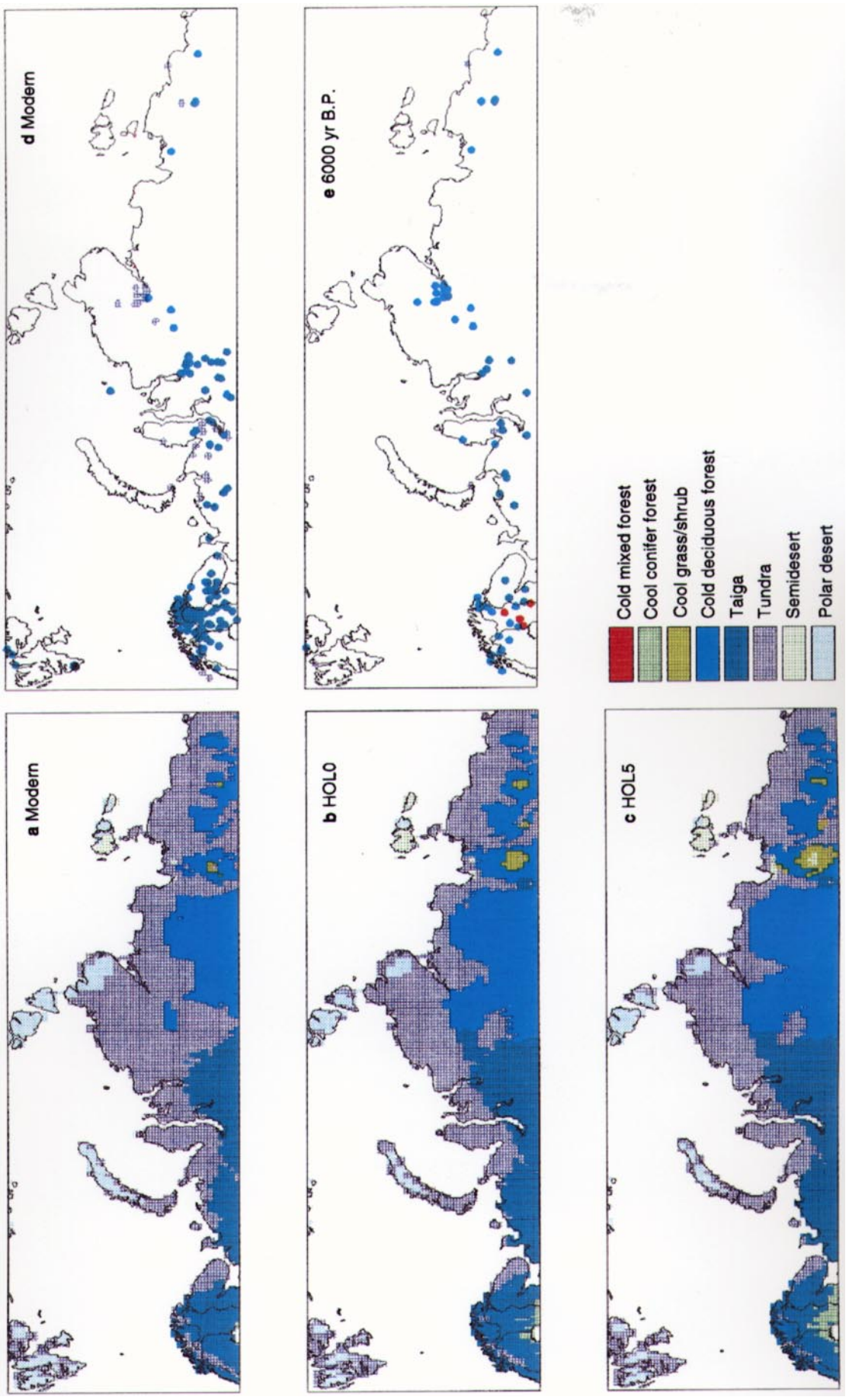

Fig. 7a–e. Simulated and observed vegetation of northern Eurasia (65–90 °N, 0–170 °E). Simulated: **a** modern, based on climatological data (Leemans and Cramer 1991); **b** from experiment HOL0, based on 6000 y BP orbital conditions and present vegetation; **c** from experiment HOL5, based on 6000 y BP orbital conditions and vegetation from HOL4. Observed: **d** modern; **e** 6000 y BP, reconstructed from pollen and/or macrofossil data at specific sites

it is still insufficient to capture the full extent of the observed changes. For example, the data show forest at several sites on the Yamal and Taymyr peninsulas up to 2–3° beyond the position of the simulated boundary of forest. The currently available data from northern Eurasia do not yet permit us to evaluate the realism of the simulated expansion of cold grass/shrub.

4.2 Northern Africa

The lake data show conditions significantly wetter than present across the Sahara (Fig. 8e). This is consistent with the occurrence of warm grass/shrub or xerophytic woods/scrub at several sites in regions now occupied by desert (Fig. 8a, d). Further south, on the coast of West Africa, the trend towards wetter conditions was registered by the replacement of warm grass/shrub and xerophytic woods/scrub by tropical dry forest/savanna.

According to the simulated biome maps, orbital changes produce a northward shift in the position of the southern margin of the desert (HOL0: Fig. 8b) in response to the simulation of a more positive water balance than present. The northward shift is greatest in the region east of Lake Chad. The shift towards wetter conditions is also registered by a northward shift of xerophytic woods/scrub and tropical dry forest. In central Africa, tropical seasonal and tropical rainforest expanded at the expense of tropical dry forest, again in response to an increase in moisture. The incorporation of vegetation feedbacks results in a further increase in *P-E* south of about 15 °N (Fig. 8f) and a further northward migration of the vegetation belts in northern Africa (HOL5: Fig. 8c). In contrast to HOL0, the largest changes in vegetation distribution occur in West Africa.

The simulations significantly underestimate the extent of wetter conditions in northern Africa in response to orbital forcing. However, to the south of about 15 °N there is reasonable agreement between the observed climate and vegetation and that simulated in response to orbital forcing. The incorporation of vegetation feedbacks produces an enhancement and extension of the region of more positive moisture balance. South of about 15 °N, this enhancement is sufficient to produce an improved match to the data. For example, the northward shift of vegetation zones on the coasts of West Africa in response to orbital forcing is insufficient to produce tropical dry forest at the sites which registered such conditions at 6000 y BP, but the additional effects of vegetation feedbacks lead to the simulation of xerophytic woods/scrub and tropical dry forest at these sites. However, north of about 15 °N, the extension of wetter conditions in response to vegetation feedbacks is too limited to correct the mismatch between simulated climate and the biome and lake data.

5 Discussion and conclusion

In response to changes in the Earth's orbital parameters at 6000 y BP, the LMD AGCM produces warmer summers and cooler winters in the NH, drier summer conditions in the mid-latitudes and an enhancement of the Afro-Asian summer monsoons. In response to these climatic changes, the tundra-forest boundary was shifted northwards, grasslands expanded at the expense of temperate and boreal forests, there was a shift from cold to warm grasslands in the mid-latitudes, and the NH deserts were reduced. The inclusion of vegetation feedbacks produces an amplification of the orbitally induced summer climate and vegetation changes both at high northern latitudes and in the African monsoon region. Comparative analyses of the sensitivity of the atmosphere/biosphere system to the two forcings suggest that, for these two regions, the climate response to vegetation forcing is generally somewhat smaller than the sensitivity to orbital forcing. Thus, the change in summer and winter temperatures in the zone north of 55 °N are respectively $+0.42$ °C and $+0.28$ °C in response to vegetation forcing alone compared to $+1.70$ °C and -0.54 °C for orbital forcing alone. The change in summer precipitation along the southern margin of the Sahara is $+0.82\ \mathrm{mm\,day^{-1}}$ in response to orbital forcing and $+0.61\ \mathrm{mm\,day^{-1}}$ in response to vegetation feedbacks.

The changes in regional climates simulated by the LMD AGCM in response to orbital changes are comparable to other published 6000 y BP simulations (e.g. Kutzbach and Guetter 1986; Kutzbach et al. 1993; Mitchell 1993; Liao et al. 1994; de Noblet et al. 1996b; Hall and Valdes 1997; Hewitt and Mitchell 1996; Kutzbach et al. in press), as are the resulting changes in vegetation (e.g. Kutzbach et al. in press; TEMPO Members 1996; Harrison et al. (in press). Differences in the magnitude of the vegetation response to orbital forcing as simulated by AGCMs with prescribed oceans are rather small at a zonal scale. Harrison et al. (in press), for example, showed that the area of tundra north of 30 °N simulated with BIOME1 driven by output from several PMIP AGCM simulations was reduced to between 74–83% of its modern extent; in the HOL0 experiment, this value is 78%.

Our simulations are made with fixed, modern SSTs. Simulations with computed SSTs show that sea-ice feedbacks can amplify the effects of orbital forcing in the high northern latitudes (Kutzbach and Gallimore 1988; Mitchell et al. 1988). However, the incorporation of a mixed-layer ocean leads to much larger differences between GCMs in the simulated magnitude of the vegetation response to 6000 y BP orbital forcing, with a reduction in the area of tundra of between 70% and 97% of its modern extent, than are observed between the same AGCMs run with fixed SSTs (TEMPO Members 1996). It therefore seems premature to rely on these models in experiments designed to isolate the climate response to vegetation feedbacks.

The effects of the incorporation of vegetation feedbacks on high northern latitude climates have been previously examined by Foley et al. (1994). They used version 1 of GENESIS AGCM coupled to a mixed-layer ocean to simulate the effects of expanding the northern boreal forests to the Arctic coast. The prescribed change led to a warming of 3–4 °C in spring and 1.6 °C in the annual average in the zone between 60–90°N: values significantly larger than those obtained in our experiments and which would suggest that vegetation feedbacks are significantly

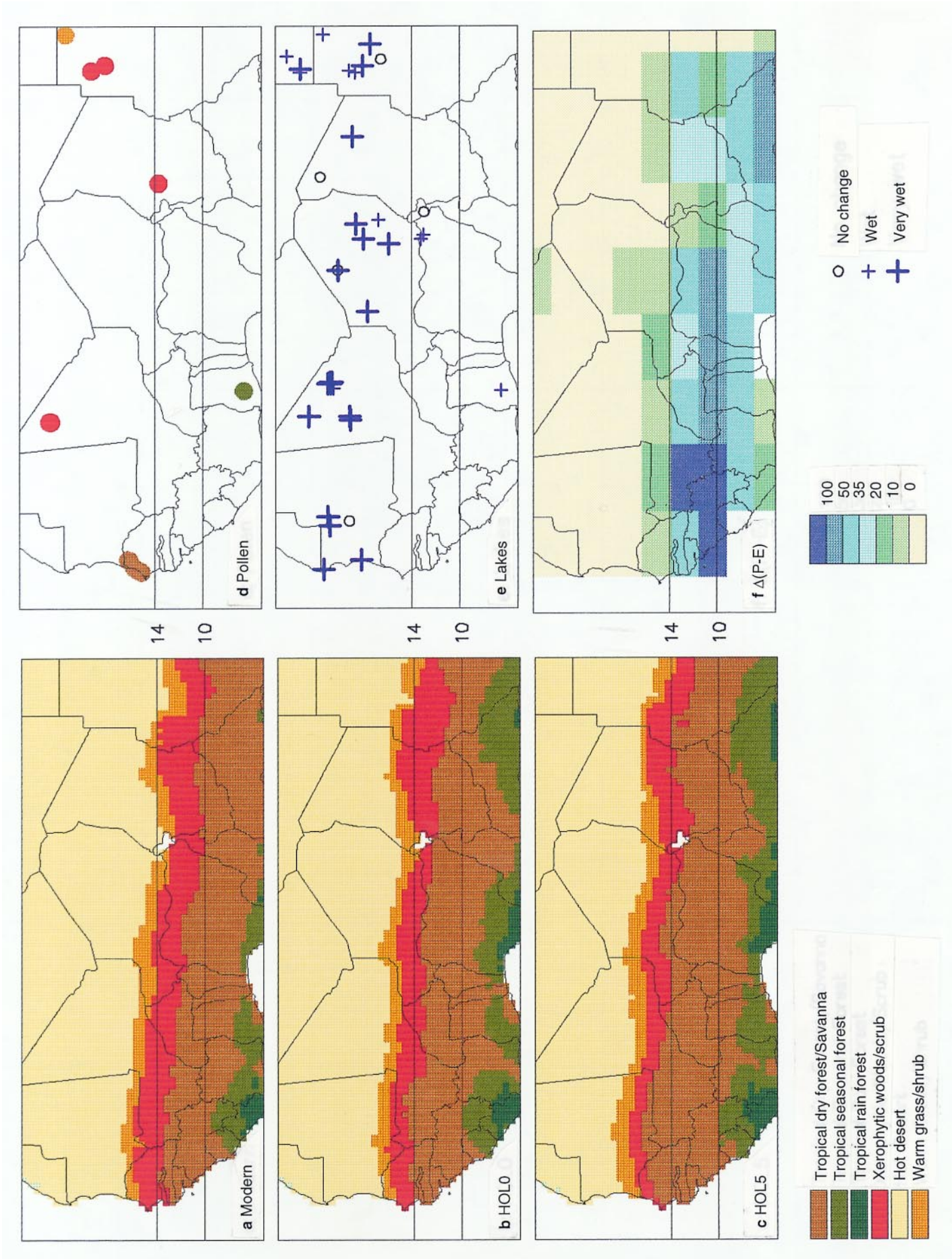
a Modern
b HOL0
c HOL5
d Pollen
e Lakes
f Δ(P-E)
14
10
Tropical dry forest/Savanna
Tropical seasonal forest
Tropical rain forest
Xerophytic woods/scrub
Hot desert
Warm grass/shrub
No change
Wet
Very wet
100
50
35
20
10
0

more important determinants of high-latitude climates than we estimate. The prescribed change in the extent of the northern boreal forests in Foley et al.'s (1994) experiments is much bigger than the change simulated in our (and other) experiments in response to orbital changes, and probably about twice as big as the observed change at 6000 y BP (TEMPO Members 1996). Thus, the actual magnitude of the boreal forest feedback on temperature may have been smaller than suggested by Foley et al. (1994). It is important to investigate how strongly nonlinear the relationship between changes in the extent of boreal forest and the consequent warming is, in order to determine whether this provides a complete explanation for the discrepancy between our results and those obtained by Foley et al. (1994). The use of a mixed-layer ocean may also contribute to the discrepancy between our results and those of Foley et al. (1994).

The effects of the incorporation of vegetation feedbacks on the African monsoon has previously been examined by Kutzbach et al. (1996) and Claussen and Gayler (in press). Kutzbach et al. (1996) used version 2 of the NCAR Community Climate Model (CCM2) which includes a land-surface model (LSM) with an explicit treatment of vegetation and soil processes to examine the effects of changing the vegetation between 15–30 °N from desert to grassland. The prescribed change leads to an enhancement of summer precipitation in the eastern Sahara (between 15–22 °N and from 0–50 °E) of 6% compared to an increase of 12% as a consequence of orbital forcing alone. The relative importance of orbital forcing and vegetation feedbacks in this experiment is about the same as obtained in our simulations, although the rainfall value for the control run is about twice as large in CCM2 than in the LMD AGCM, while the initial increase in summer precipitation simulated by the CCM2 is considerably less than the increase simulated for this region in HOL0. In our experiments, orbital forcing increases rainfall by 60% and vegetation feedbacks further increase rainfall by 30%. Claussen and Gayler (in press) used the ECHAM model asynchronously coupled to BIOME1. As in our experiments, the coupled model produces a significant enhancement of monsoon precipitation over northern Africa. Although, the orbitally induced change in rainfall simulated by the ECHAM model is smaller than the change obtained in HOL0, Claussen and Gayler (in press) were able to produce a much larger amplification of the monsoon as a result of vegetation feedbacks such that the southern limit of Sahara was pushed to approximately 20 °N after 3 iterations whereas the southern limit of the Sahara is only pushed to approximately 18 °N after 5 iterations (HOL5) in our experiments. An intercomparison study is currently underway to examine the reasons for this discrepancy .

The response to vegetation feedbacks can exceed the sensitivity to orbital forcing in certain seasons and regions. One such region is West Africa, where our results suggest that vegetation feedbacks more than doubles the increase of summer precipitation produced by 6000 y BP orbital forcing. The absence of significant change in the extent of the monsoon over West Africa has been a persistent feature of AGCM simulations of mid-Holocene climates (Jolly et al. in press; Harrison et al. (in press). Changes in the ocean sea-surface temperature off the West African coast can produce a significant increase in monsoon precipitation onshore (J. E. Kutzbach and Z. Liu personal communication 1996). Our results and those of Claussen and Gayler (in press) suggest that vegetation feedbacks may also enhance monsoon precipitation in this region. The incorporation of more accurate land and ocean-surface conditions, or the use of coupled vegetation and ocean models, could therefore be necessary to provide a fully realistic simulation of the 6000 y BP climate of West Africa.

Pollen data indicate that, despite the lower insolation, high-latitude winters in Europe were warmer during the mid-Holocene than today (Huntley and Prentice 1993; Cheddadi et al. 1996). This situation can be explained by the fact that direct effects of orbital changes may be moderated by indirect effects, including changes in oceanic heat advection consequent on changes in atmospheric circulation and/or sea-ice feedbacks (Harrison et al. 1992). Vegetation feedbacks may also play a role in moderating the effect of orbital changes on seasonal climates. The orbital forcing at 6000 y BP enhances the seasonal contrast in the NH, leading to warmer summers and cooler winters. Vegetation forcing, however, tends to act in the same direction throughout the year. In the high-northern latitudes, for example, vegetation feedbacks lead to a year-round warming thus enhancing orbital changes in summer and opposing them in winter. Although our experiments do not produce winters warmer than present in the high-latitudes of Europe or northern Eurasia, they do show winters warmer than present over much of northern Canada.

Although incorporation of vegetation feedbacks amplifies both high-latitude warming and monsoon precipitation, it is still not sufficient to eliminate the differences between observed and simulated climate and vegetation in northern Eurasia and northern Africa. This is doubtless a reflection of the absence of other relevant feedbacks, including changes in ocean and other land-surface conditions. Sensitivity experiments suggest that the African monsoon may be more sensitive to changes in soil properties (albedo and available water holding capacity) caused by changes in vegetation than to the vegetation change itself (Kutzbach et al. 1996). Other factors that could lead to a further enhancement of the African monsoon include the changes in the ocean sea-surface temperature to the west of northern Africa (Kutzbach and Liu unpublished data) such as those induced by changes in the strength of upwelling. In the absence of fully coupled models of these sub-systems, it would be appropriate to see whether the

Fig. 8a–f. Simulated and observed climate and vegetation of northern Africa (5–25 °N, 20 °W–30 °E). Simulated: **a** modern, based on climatological data (Leemans and Cramer 1991); **b** from experiment HOL0, based on 6000 y BP orbital conditions and present vegetation; **c** from experiment HOL5, based on 6000 y BP orbital conditions and vegetation from HOL4. Observed: **d** 6000 y BP vegetation reconstructed from pollen data at specific sites (from Jolly et al. in press); **e** changes in lake status at 6000 y BP reconstructed from geomorphic and biostratigraphic evidence (from Jolly et al. in press); **f** change in annual P–E simulated in response to the combined orbital and vegetation forcings (HOL5-Ctrl)

incorporation of a realistic prescription of ocean and land-surface conditions across northern Africa at 6000 y BP is sufficient to improve the match between simulated and observed monsoon climates. Since sea-ice feedbacks undoubtedly played an important role in mid-Holocene climate changes in the high-latitudes, our experiments could be repeated with a mixed-layer ocean model. However, given the large range in the response of mixed-layer ocean simulations to orbital forcing (TEMPO Members 1996), it will be important to undertake such studies in the context of systematic model intercomparison such as those being undertaken by PMIP.

Acknowledgements. We warmly thank Pascale Braconnot and Valérie Masson for constructive discussions on this study, and the reviewers who helped improve the manuscript. This work is a contribution to the GAIM 6000 y BP experiment, supported by the Environmental Protection Agency via a subcontract from the University of New Hampshire, UK and was supported by the European Community (EV5V-CT94-0457), by the Swedish Natural Science Council (G-AA/GU 09334-321) and by the Crafoord Fund (The role of sea-ice and vegetation feedbacks in the last interglacial and mid-Holocene climates of northern Eurasia).

References

Adams JM, Faure H, Faure-Denard L, McGlade JM, Woodward FI (1990) Increases in terrestrial carbon storage from the Last Glacial Maximum to the present. Nature 348 : 711–714

Berger A (1978) Long-term variation of daily insolation and Quaternary climatic changes. J Atmos Sci 35(12) : 2362–2367

Berger A (1988) Milankovitch theory and climate. Rev Geophys 26(4) : 624–657

Bolikhovskaya NS, Bolikhovskii VF, Klimanov VA (1988) Klimaticheskie i kryogennye faktory razvitiya torfiannikov evropeiskogo severo-vostoka SSSR *v* golotsene, In: Khotinskii NA, Klimanov VA (eds) Paeoklimaty golotsena, evropeiskoi territorii SSSR. Moscow: Inst. Geographii AN SSSR, pp 36–44

Bonan GB, Pollard D, Thompson SL (1992) Effects of boreal forest vegetation on global climate. Nature 359 : 716–718

Broccoli AJ, Marciniak EP (1996) Comparing simulated glacial climate and paleodata: a reexamination. Paleoceanography, 11(1) : 3–14

Chalita S, Le Treut H (1994) The albedo of temperate and boreal forests and the northern hemisphere climate: a sensitivity experiment using the LMD GCM. Clim Dyn 10 : 213–240

Cheddadi R, Yu G, Guiot J, Harrison SP, Prentice IC (1996) The climate of Europe 6000 years ago. Clim Dyn 13 : 4–9

Claussen M (1994) On coupling global biome models with climate models. Clim Res 4 : 203–221

Claussen M (1996) Variability of global biome patterns as a function of initial and boundary conditions in a climate model. Clim Dyn 12 : 371–379

Claussen M, Gaylor V (1997) The greening of Sahara during the mid-Holocene: results of an interactive atmosphere-biosphere model. Global Ecol Biogeogr Let (in press)

COHMAP Members (1988) Climatic changes of the last 18000 years: observations and model simulations. Science 241 : 1043–1052

Crowley TJ (1995) Ice-Age terrestrial carbon changes revisited. Glob Biogeochem Cycles 9 : 377–389

Davydova NN, Delusina IV, Subetto DA (1992) Boltshezemeltskaya tundra. In: Davydova NN (ed) Istoriya ozer Vostochno-Evropeiskoi ravniny. St. Petersburg: Nauka pp 35–45

Ducoudré N, Laval K, Perrier A (1993) SECHIBA, a new set of parametrizations of the Hydrologic exchanges at the land-atmosphere interface within the LMD atmospheric general circulation model. J Clim 6(2) : 248–273

Elina GA, Filimonova LV, Klimanov VA (1995) Late glacial and Holocene paleogeography of East Fennoscandia. In: Velichko AA (ed) Climate and environmental changes of East Europe during Holocene and Late-Middle Pleistocene. Moscow: Institute of Geography RAS: pp 20–27

Federer CA (1968) Spatial variation of net radiation, albedo and surface temperature of forests. J Appl Meteorol 7 : 789–795

Firsov LV, Panychev VA, Orlova LA (1972) Radiouglerodnye daty laboratorii geokhronologii Instituta geologii i geofiziki SO AN SSSR, Novosibirk. Byull Kom Izuch Chetvertichn Perioda 38 : 190–197

Foley J, Kutzbach JE, Coe MT, Levis S (1994) Feedbacks between climate and boreal forests during the Holocene epoch. Nature 371 : 52–54

Fouquart Y, Bonnel B (1980) Computations of solar heating of the Earth's atmosphere: a new parametrization. Beitr Phys Atmos 53 : 35–62.

Gates W (1992) The atmospheric model intercomparison project. Bull Am Meteorol Soc 73 : 1962–1970

Hall NMJ, Valdes PJ (1997) A GCM simulation of the climate 6000 years ago. J Clim 10 : 3–17

Harrison SP, Jolly D, Laarif F, Abe-Ouchi A, Herterich K, Hewitt C, Joussaume S, Kutzbach JE, Mitchell J, de Noblet N, Valdes P (1997): Intercomparison of simulated global vegetation distribution in response to 6kyr BP orbital forcing. J Clim (in press)

Harrison SP, Kutzbach JE, Prentice IC, Behling P, Sykes MT (1995) The response of Northern Hemisphere extratropical climate and vegetation to orbitally-induced changes in insolation during the last intergalcial: results of atmsopheric general circulation model and biome simulations. Quat Res 43 : 174–184

Harrison SP, Prentice IC, Bartlein PJ (1992) Influence of insolation and glaciation on atmospheric circulation in the North Atlantic sector: implications of general circulation model experiments for the Late Quaternary climatology of Europe. Quat Sci Rev 11 : 283–299

Harzallah A, Sadourny R (1995) Internal versus SST forced atmospheric variability as simulated by an atmospheric general circulation model. J Clim 8 : 474–498

Haxeltine A and Prentice IC (1996) BIOME3: an equilibrium biosphere model based on ecophysiological constraints, resource availability and competition among plant functional types. Global Biochem Cycl 10 : 693–709

Henderson-Sellers A (1993) Continental vegetation as a dynamic componant of a global climate model: a preliminary assessment. Clim Change 23 : 337–377

Hewitt CD, Mitchell JFB (1996) GCM simulations of the climate of 6ky BP: mean changes and interdecadal variability. J Clim 9 : 3505–3529

Huntley B, Prentice IC (1993) Holocene vegetation and climates of Europe. In: Wright Jr HE, Kutzbach JE, Webb III T, Ruddiman WF, Street-Perrott FA, Bartlein PJ (eds) Global climates since the Last Glacial Maximum. University of Minnesota Press, Minneapolis: pp 136–168

Hyvärinen H (1976) Flandrian pollen deposition rates and tree-line history in northern Fennoscandia. Boreas 5 : 163–175

Jolly D, Harrison SP, Damnati B, Bonnefille R (1996) Simulated climate and biomes of Africa during the Late Quaternary: comparison with pollen and lake status data. Quat Sci Rev (in press)

Joussaume S, Braconnot P (1996) Sensitivity of paleoclimate simulation results to season definition. J Geophys Res 102 (D2), 1943–1956

Joussaume S, Taylor K (1995): Status of the Paleoclimate Modeling Intercomparison Project (PMIP). Proc AMIP Conf (WCRP), Monterey, USA

Kagan LYa, Koshechkin BI, Lebedeva RM (1992) Kolskii poluostrov. In: Davydova NN (ed) Istoriya ozer Vostochno-Evropeiskoi ravniny. St Petersburg, Nauka, 20–34

Kaplina TA, Lozhkin AV (1979) Vozrast alasnykh otlozhenii primorskoi nizmennosti Yakutii. Izvestiya AN SSSR, Geologiya 2 : 69–76

Kind NV (1974) Geokhronologiya pozdnego antropogena po izotopnym dannym. Nauka, Moscow, 255pp

Kuo HL (1965) On the formation and intensification of tropical cyclones through latent heat release by cumulus convection. J Atmos Sci 22 : 40–63

Kutzbach JE, Guetter PJ (1986) The influence of changing orbital parameters and surface boundary conditions on climate simulations for the past 18 000 years. J Atmos Sci 43 : 1726–1759

Kutzbach JE, Gallimore RG (1988) Sensitivity of a coupled atmosphere/mixed-layer ocean model to changes in orbital forcing at 9000 years BP. J Geophys Res 93 : 803–821

Kutzbach JE, Guetter PJ, Behling PJ, Selin R (1993) Simulated climatic changes: results of the COHMAP climate-model experiments. In: Wright Jr HE, Kutzach JE, Webb III T, Ruddiman WF, Street-Perrott FA, Bartlein PJ (eds) Global climates since the Last Glacial Maximum. University of Minnesota Press, Minneapolis: pp 24–93

Kutzbach JE, Bonan G, Foley J, Harrison SP (1996) Vegetation/soil feedbacks and African monsoon response to orbital forcing in the Holocene. Nature 384 : 623–626

Kutzbach JE, Gallimore RG, Harrison SP, Behling PJ, Selin, Laarif F (1997) Climate simulations for the past 21 000 years. Quat Sci Rev (in press)

Lavrushin Yu A, Devirts AL, Giterman RE, Markova NG (1963) Pervye dannye ob absolyutnoi chronologii osnovnykh sobytii golotsena Severo-Vostoka SSSR. Byull Kom Izuch Chetvertichn Perioda 28 : 112–126

Leemans R, Cramer W (1991) The IIASA climate database for mean monthly values of temperatures, precipitation and cloudiness on a terrestrial grid. RR-91-18, IIASA, Laxenburg

Levkovskaya GM, Kind NV, Zaveltskii FS, Forova VS (1970) Absolutnyi vozrast torfiannikov raiona g. Igarka i raschlenenie golotsena Zapadnoi Sibiri. Byull Kom Izuch Chertvertichn Perioda 37 : 94–101

Liao X, Street-Perrott FA, Mitchell JFB (1994) GCM experiments with different cloud parameterization: comparisons with palaeoclimatic reconstructions for 6000 years BP. Palaeoclim: Data Modell 1 : 99–123

Lozhkin AV (1993) Geochronology of late Quaternary events in Northeastern Russia. Radiocarbon 35 : 429–433

Malyasova ES, Serebriannyl ER (1993) Estestvennaya istoriya Novoi Zemli. In: Boyarskii, PV (ed) Novaya Zemlia 2. Moscow: 10–22

Manabe S, Stricker RF (1964) Thermal equilibrium of the atmosphere with a convective adjustment. J Atmos Sci 21 : 361–385

Maslin MA, Adams J, Thomas E, Faure H, Haines-Young R (1995) Estimating the carbon transfer between the ocean, atmosphere and the terrestrial biosphere since the last glacial maximum. Terra Nova 7 : 358–366

Masson V, Joussaume S (1997) Energetics of Mid-Holocene atmospheric circulation change in boreal summer from large scale to monsoon areas: a study with two versions of the LMD AGCM. J Clim (in press)

Mitchell JFB, Graham NS, Needham KJ (1988) Climate simulations for 9000 years before present: seasonal variations and effects of the Laurentide ice sheet. J Geophys Res 93 : 8283–8303

Mitchell JFB (1993) Modelling of paleoclimates: examples from the recent past. Philos Trans R Soc London 341 : 267–275

Morcrette JJ (1991) Radiation and cloud radiative properties in the ECMWF operational weather forecast model. J Geophys Res 96 : 9121–9132

de Noblet N, Braconnot P, Joussaume S, Masson V (1996a) Sensitivity of simulated Asian and African summer monsoons to orbital induced variations in insolation 126, 115 and 6 kBP. Clim Dyn 12 : 589–603

de Noblet N, Prentice IC, Joussaume S, Texier D, Botta A, Haxeltine A (1996b) Possible role of atmosphere-biosphere interactions in triggering the last glaciation. Geophys Res Lett 23(22) : 3191–3194

Nikol'skaya MV (1982) Paleobotanicheskie i paleoklimaticheskie rekonstruktsii golotsena Taimyra. In: Antrpogen Taimyra. Moscow, Nauka, pp 148–157

Nikol'skaya MV, Cherkasova MN (1982) Dinamika golotsenovykh flor Taimyra paleofitologicheskim I geokhronologischeskim dannym). In: Razvitic priroly territorii SSSR v pozdem pleistotsene I golotsene. Moscow, Nauka, pp 192–204

Parunin OB, Timashkova TA, Turchaninov PS, Shlukov AI (1984) Spisok radiouglerodnykh datirovok laboratorii Noveishikh otlozhenii i paleografii pleistotsena geograficheskogo fakultteta MGU (soobshchenie X). Byull Kom Izuch Chetvertichn Perioda 53 : 169–172

Petit-Maire N, Page N (1992) Remotes sensing and past climatic changes in tropical deserts: example of the Sahara. Episodes 15 : 113–117

Prentice IC, Cramer W, Harrison SP, Leemans R, Monserud RA, Solomon AM (1992) A global biome model based on plant physiology and dominance, soil properties and climate. J Biogeogr 19 : 117–134

Prentice IC, Sykes MT, Lautenschlager M, Harrison SP, Denissenko O, Bartlein PJ (1993) Modelling the increase in terrestrial carbon storage after the last glacial maximum. Glob Ecol Biogeogr Lett 3 : 67–76

Prentice IC, Guiot J, Huntley B, Jolly D, Cheddadi R (1996) Reconstructing biomes from palaeoecological data: a general method and its application to European pollen data at 0 and 6 ka. Clim Dyn 12 : 185–194

Raynaud D, Jouzel J, Barnola J, Chappelaz J, Delmas R, Lorius C (1993) The ice record of greenhouse gases. Science 259 : 926–934

Ritchie JC (1987) The postglacial vegetation of Canada. Cambridge University Press, Cambridge, 187pp

Sadourny R, Laval K (1984) January and July performance of the LMD general circulation model. In: Berger A, Nicolis C (eds). New perspectives in climate modelling. Elsevier, Amsterdam, pp 173–198

Shilo NA, Bespalyi VG, Davydovich TD et al. (1971) Obzor radiouglerodnykh datirovok verkHOL5pleistotsenovykh i golotsenovykh otlozhenii Severo-Vostoka Azii. Geol Geofiz 10 : 13–24

Street FA, Grove AT (1976) Environmental and climatic implications of late Quaternary lake-level fluctuations in Africa. Nature 261 : 385–390

Street-Perrott FA, Mitchell JFB, Marchand DS, Brunner JS (1990) Milankovitch and albedo forcing of the tropical monsoons: a comparison of geological evidence and numerical simulations for the 9000 y BP. Trans R Soc Edinburgh: Earth Sci 81 : 407–427

Street-Perrott FA, Perrott RA (1993) Holocene vegetation, lake levels and climate of Africa. In: Wright Jr HE, Kutzbach JE, Webb III T, Ruddiman WF, Street-Perrott FA, Bartlein PJ (eds) Global climates since the Last Glacial Maximum. University of Minnesota Press, Minneapolis, pp 318–356

Tarasov PE, Pushenko MYa, Harrison SP, Saarse L, Andreev AA, Aleshinskaya ZV, Davydova NN, Dorofeyuk NI, Efremov YuV, Elina GA, Elovicheva YaK, Filimonova LV, Gunova VS, Khomutova VI, Kvavadze EV, Neustreuva IYu, Pisareva VV, Sevastyanov DV, Shelekhova TS, Subetto DA, Uspenskaya ON, Zernitskaya VP (1996) Lake status records from the former Soviet Union and Mongolia. Documentation of the second version of the Database. NOAA Paleoclimatology Publications Series Rep 5, 224 pp

TEMPO Members (1996) Potential role of vegetation feedback in the climate sensitivity of high-latitude regions: a case study at 6000 years B.P. Glob Biogeochem Cycl 10(4) : 727–736

Ukraintseva VV (1991) Istoriya biogeotsenozov Taimyra za poslednie 55 tysiach let. Bot Zh 76(9) : 1308–1316

Vasil'chuk K Yu, Petrova EA, Serova AK (1983) Nekotorye cherty oakeogeografii golotsena Yamaia. Byull Kom Izuch Chetvertichn Perioda 52 : 73–89

Veinbergs IG, Stelle VYa, Savvaitov AS, Yakubovska IYa (1995) PozdnechetverticHOL1ya istoriya razvitiya poberezhya Pechorskogo moria. In: Svitoch AA (ed) Korreliatsiya paleogeographicheskikh sobytii: mazteric-sheltf-okean. Moscow. Izdateltstvo Moskovskogo Universiteta, pp 106–112

Velichko AA et al. (1992) Atlas of Paleoclimates and Paleoenvironments of the Northern Hemisphere: Late Pleistocene – Holocene. Frenzel B, Pécsi M, Velichko AA (eds) Geographical Research Institute, Hungarian Academy of Sciences, Budapest

Velichko AA, Andreev AA, Klimanov VA (1994) Dinamika rastiteltnosti I klimata v tundrovoi i lesnoi zonakh Severnoi Evrazii v pozdnelednikovte I golotsene. In: Korotkoperiodnye i rezkie landshaftno-klimaticheskie izmeneniya za poslednie 15000 let. Moscow: Institute of Geographii RAN, pp 4–60

Winkler MG, Wang PK (1993) The Late-Quaternary vegetation and climate of China. In: Wright Jr HE, Kutzbach JE, Webb III T, Ruddiman WF, Street-Perrott FA, Bartlein PJ (eds) Global climates since the Last Glacial Maximum. University of Minnesota Press, Minneapolis, pp 221–264

Yu G, Harrison SP (1996) An evaluation of the simulated water balance of Eurasia and northern Africa at 6000 y BP using lake status data. Clim Dyn 12(11): 723–735